ELSEVIER

Journal of Power Sources 61 (1996) 173–181

JOURNAL OF POWER SOURCES

Performance/structure correlation for composite SOFC cathodes

Mette Juhl, Søren Primdahl, Carrie Manon, Mogens Mogensen

Materials Department, Risø National Laboratory, 4000 Roskilde, Denmark

Abstract

Many solid oxide fuel cell (SOFC) developers use composite electrodes. The cathode is often a mixture of La(Sr)MnO_3 and yttria stabilised zirconia (YSZ). Two kinds of cathode structure were studied by means of impedance spectroscopy and d.c. electrochemical methods. The measurements were performed in air at 700–1000 °C. Then, the electrode microstructures were examined ceramographically. The cathode performance was improved by increasing the thickness of the composite electrode, and the polarisation resistance was decreased by extending the active triple phase boundary line through the application of a coarse layer of YSZ particles on the electrolyte surface before the composite cathode was applied. The performance proved to be sensitive to structural changes at 700 and 850 °C, whereas the effect of the structure was limited at 1000 °C. Values as low as 0.07 Ω cm^2 at 1000 °C and 0.50 Ω cm^2 at 850 °C were obtained in air at an overvoltage of −50 mV. Two simple models relating performance, percolation and triple phase boundary length were used for the interpretation of the results and for assessing the potential for further improvement of the performance by optimising the microstructure.

Keywords: Solid oxide fuel cells; Cathodes; Lanthanum strontium manganite; Yttria stabilised zirconia; Structure; Performance

1. Introduction

The structure of the porous electrodes is critical for the performance of a solid oxide fuel cell (SOFC). The traditional materials used in SOFCs are strontium-doped lanthanum manganite (LSM) as the cathode, yttria stabilised zirconia (YSZ) as the electrolyte and a NiO/YSZ composite as the anode. The present work investigates the correlation between the structure and the performance of a composite SOFC cathode consisting of LSM and YSZ.

In an SOFC the reaction at the air electrode is the following (Kröger Vink notation used Ref. [1]):

$$O_2(g) + 4e'_{electrode} + 2V_{O,electrolyte}^{\cdot\cdot} \rightleftarrows 2O_{O,electrolyte}^{x} \quad (1)$$

where e' is an electron from the electrode. $V_O^{\cdot\cdot}$ and O_O^x symbolise an oxide ion vacancy and an oxide ion in the crystal lattice of the electrolyte, respectively. This reaction requires the presence of oxygen and electrons as well as the possibility for created oxide ions to be transported from the reaction site into the bulk of the electrolyte. As both the ionic conductivity of LSM and the electronic conductivity of YSZ are low, these criteria are only fulfilled in the vicinity of the triple phase boundary (TPB) between the electrode, electrolyte and air. However, the TPB is only electrochemically active if electrons, oxide ions and gas can percolate freely through LSM, YSZ and pores, respectively, to and from the TPB. Since the microstructure determines the extent of active TPB, the reaction rate depends on the microstructure [2–8].

Several authors have studied lanthanum manganite electrodes [2–6]. Mizusaki and co-workers [2,3] have investigated $La_{0.6}Ca_{0.4}MnO_3$ electrodes painted on a YSZ substrate. Using rather coarse particles (1–3 μm) the reaction rate was essentially independent of the electrode thickness and was proportional to the TPB length [2]. This implies a close relationship between the electrode morphology and its performance [3].

The correlation between structure and performance for a $La_{0.85}Sr_{0.15}MnO_3$ cathode screen printed on YSZ was studied at 800 °C by Sasaki et al. [4]. They found that the performance correlated with the length of TPB and the electrode thickness. At 800 °C a minimum in area specific polarisation resistance, R_p, was found for a cathode thickness of 25 μm. Electrodes manufactured from LSM with a narrow particle size distribution (PSD) had a low R_p compared with electrodes manufactured from powder with a wide PSD. A similar effect was observed by van Heuveln et al. [5] with $La_{0.85}Sr_{0.15}MnO_3$ electrodes on YSZ in oxygen at 920 °C. Additionally, van Heuveln et al. observed that powder with a narrow PSD, calcined at high temperature before electrode manufacture, had an R_p which exceeded the value for an electrode with a wide PSD.

In contrast, de Haart et al. [6] found that the polarisation behaviour of an $La_{0.85}Sr_{0.15}MnO_3$ electrode produced by a

PII S0378-7753(96)02361-0

dip coat process was not significantly dependent on the electrode microstructure and thickness. This, in relation with Refs. [2–5], indicates that the electrode performance is closely related to the techniques used for powder processing and electrode manufacturing.

Using composite electrodes made from a mixture of electronic and ionic conductive materials, as in the present work, tends to complicate things. Kenjo and Nishiya [7] investigated composite electrodes of YSZ and La_xMnO_3 with varying weight ratios of the two components. The electrodes were manufactured by painting a turpentine-based slurry on an electrolyte disk and iso-statically pressing the green electrode. The polarisation behaviour was measured at 900 °C in air. The authors found that additional reaction sites were created inside the composite electrodes. The addition of 50 wt.% YSZ to an $La_{0.85}MnO_3$ electrode decreased the R_p from 0.77 to 0.16 Ω cm^2. Electrodes containing a 1:2 ratio of $La_{0.85}MnO_3$ and YSZ exhibited a decreasing R_p as the electrode thickness was increased.

Østergård et al. [8] investigated composite electrodes consisting of LSM and YSZ at 1000 °C in air. The electrodes were manufactured by a spray-coating technique also used in the present work. With an $(La_{0.85}Sr_{0.15})_{0.9}MnO_3$ (nominal composition) electrode an improvement of the R_p from 2.7 to 0.65 Ω cm^2 was found by the addition of 20 wt.% fine-grained YSZ. Østergård et al. found the structure of the composite electrode to be of major importance with respect to performance. Composite electrodes made with a mixture of fine and coarse LSM had a lower resistance than these electrodes containing either fine or coarse LSM powder. The best result in this work, $R_p = 0.5$ Ω cm^2, was obtained with a composite electrode containing 40 wt.% YSZ.

2. Experimental

The composite electrodes investigated in the present work consist of two layers: (i) the electrochemical active cathode layer (C-layer), and (ii) the cathode current collecting layer (CCC-layer). The C-layer which is applied directly on the electrolyte surface is a composite of LSM and YSZ. The thickness of this layer is in the range of 2 to 12 μm. To ensure that current is collected from the whole electrode area a porous CCC-layer of LSM, approximately 40 μm thick, is attached to the C-layer. In principle, the CCC-layer is electrochemically inactive. However, since the CCC-layer covers the surface and fills voids and cracks in the C-layer, thus contacting a number of YSZ grains, some contribution to the TPB is expected. The application method used is spray-coating, a simple method with a large scale-up potential.

The composition of the LSM used for the C-layer and the CCC-layer is $(La_{0.75}Sr_{0.25})_{0.9}MnO_3$ (nominal composition). The lanthanum deficiency is believed to minimise the formation of zirconates at the interface between the electrode and electrolyte [7,9]. The chosen level of strontium doping suppresses the formation of lanthanium and strontium zirconates at this interface [10].

The present work comprises two series of samples. The effect of the C-layer thickness was investigated in series 1. In series 2 the effect of altering the microstructure of the C-layer by applying a layer of YSZ particles (P-layer) on the electrolyte surface was studied. The purpose of this layer was to obtain a more open structure of the C-layer, to improve the distribution of YSZ in the C-layer and to expand the YSZ surface area.

One aim of the SOFC research is to lower the operation temperature; the electrode performance was therefore investigated over a wide temperature range.

2.1. Preparation of powder and samples

The LSM powder was produced by the glycine nitrate process [11]. After drip pyrolysis in a rotating furnace [12] the powder was heat-treated at 600 °C for 2 h in order to remove any remaining organic compounds.

Iso-statically pressed pellets of Tosoh TZ8Y (ZrO_2 with 8 mol% Y_2O_3) were sintered at 1450 °C to a density above 99% of the theoretical value and used as the electrolyte. The shape of the electrolyte pellet is shown in Fig. 1. The area of the electrode to be investigated, the working electrode, was approximately 0.42 cm^2. The counter electrode (Fig. 1) consisted of platinum paste applied by painting, whereas the reference electrode was a platinum bead.

The working electrode was spray-coated onto the electrolyte as an ethanol-based slurry with a low viscosity. The slurry was produced by ball milling powder, solvent and dispersant. After spraying the C-layer the samples were sintered at 1300 °C for 2 h. Thereafter, two CCC-layers were applied by a similar process. Each layer was sintered at 1300 °C for 2 h.

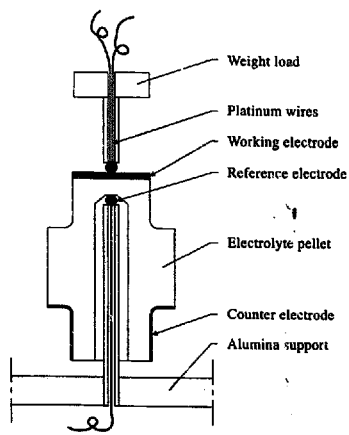

Fig. 1. Schematic of the electrochemical cell setup.

Table 1
Description of C-layer composition for series 1 and 2

Series	Sample	C-layer composition	Remarks
1	K313–K318	50 wt.% $(La_{0.75}Sr_{0.25})_{0.9}MnO_3$, mixture (1:1) of uncalcined powder and powder calcined at 1300 °C for 2 h; 50 wt.% uncalcined TZ3Y	
2	K310–K311	P-layer (YSZ particles with an average diameter of 23 μm) followed by C-layer containing 50 wt.% uncalcined $(La_{0.75}Sr_{0.25})_{0.9}MnO_3$ and 50 wt.% uncalcined TZ3Y	P-layer and C-layer co-sintered
	K319–K320	50 wt.% uncalcined $(La_{0.75}Sr_{0.25})_{0.9}MnO_3$ and 50 wt.% uncalcined TZ3Y	As K310–K311, but no P-layer

In series 1 the C-layer thickness was varied by changing the spray time.

In series 2 the P-layer slurry was applied directly onto the electrolyte pellets for two samples, K310 and K311. The slurry was made as follows: TZ8Y powder was calcined at 1500 °C for 4 h and ball-milled until a mean particle diameter of approximately 23 μm was achieved (measured by light scattering with Malvern Mastersizer equipment). The P-layer was then sprayed onto the electrolyte surface, the C-layer was sprayed on the P-layer and the two layers were co-sintered. Two other samples, K319 and K320, were made as references. They were intended to be as identical as possible to K310 and K311 but without the P-layer.

The C-layer consisted of equal amounts (by weight) of $(La_{0.75}Sr_{0.25})_{0.9}MnO_3$ (nominal composition) and Tosoh TZ3Y (ZrO_2 with 3 mol% Y_2O_3). TZ3Y, in preference to TZ8Y, has under similar conditions proved to be advantageous [13]. As shown in Table 1 the LSM powder used for the C-layer was treated differently for the two series of samples. In series 1 the LSM was a mixture of powder heat-treated at 600 °C and calcined at 1300 °C. The purpose of adding powder calcined at a high temperature was to lower the overall sinterability of the powder and to introduce larger grains. LSM with high sinterability (heat treated at 600 °C) was used in series 2 to ensure adhesion of both the P-layer and the C-layer onto the electrolyte. In both C-layer slurries the YSZ powder was uncalcined.

Fig. 2 shows the particle size distributions of the C-slurries prior to spraying. The particle size distributions were measured by light scattering and found to be bi-modal for both slurries. The slurry used for series 2 contained a large fraction of relatively small particles (mean particle size 0.4 μm). This fraction decreased when a part of the powder was calcined at a high temperature (series 1).

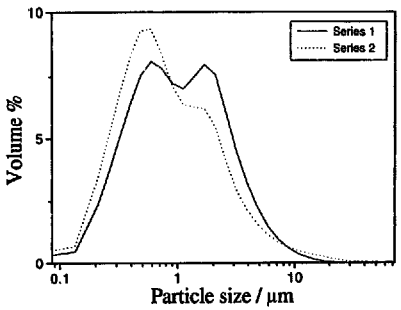

Fig. 2. Particle size distribution in the C-slurry for series 1 and series 2 measured by light scattering. (See text for details on slurry composition.)

2.2. Electrochemical characterisation

Four electrochemical cells were placed in a furnace and measurements were performed on one cell at a time. The samples were tested at three temperatures, 700, 850 and 1000 °C. The test atmosphere was air. Chrono-amperometry measurements and impedance spectroscopy measurements were performed using a Solartron 1286 potentiostat and a Solartron 1250 frequency response analyser.

Impedance measurements were taken at open-circuit voltage (OCV) and, while keeping the potential constant, after each chrono-amperometry measurement. Impedance data was typically obtained in the 65 kHz–1 mHz frequency range with an applied amplitude of 20 mV. A typical impedance plot is shown in Fig. 3. The series resistance, R_s, originating from the electrolyte is determined by the intercept of the real axis at high frequencies. R_p of the working electrode is the difference between the intercept with the real axis at low and high frequency, respectively. In practice R_s and R_p were calculated by curve fitting with the computer program EQIVCT [14].

In the chrono-amperometry measurements the current was measured at a constant potential over a 15 min period. In

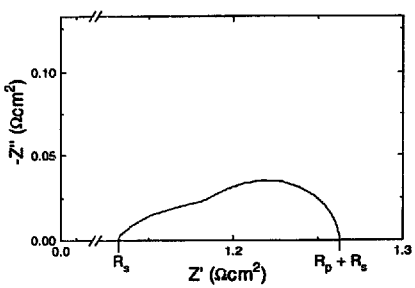

Fig. 3. Impedance plot obtained with an LSM–YSZ composite electrode (K311). The series resistance, R_s, and the area specific polarisation resistance, R_p, are indicated. Measuring conditions: OCV, 1000 °C, and air.

some cases, steady-state conditions were not fully obtained after this time period. However, all data were taken after 15 min. Chrono-amperometry measurements were performed at four different applied potentials, E, for each sample. The cathodic overvoltages, η, were calculated using Eq. (2):

$$\eta = E - iR_s \quad (2)$$

where i is the measured current density. In Fig. 4 examples of the obtained data are plotted after correction for ohmic losses. The lines are second-degree polynomials fit to the experimental data. From the second-degree polynomial the d.c. current at −50 mV overvoltage was determined and the area specific polarisation resistance calculated. At 1000 °C it was necessary to extrapolate the i–η characteristics. At this temperature the maximum applied potential was −300 mV, corresponding to cathodic overvoltages between 25 and 50 mV. Higher potentials were not applied to the sample due to the risk that the high current would cause localised heating.

2.3. Characterisation of structures

The electrochemical cells were embedded in epoxy resin before being cut and polished in order to prepare samples, to be examined by scanning electron microscopy (SEM), without damaging the structures. The C-layer thickness was determined using a computer program called PCImage. The standard deviations on the thickness measurements of 2–3 μm and 4–11 μm were 0.5–1 μm and 1–2 μm, respectively. Generalisations about the electrode structure were made by inspecting 10 to 12 micrographs taken at random locations on each sample.

3. Results and discussion

3.1. Series 1, effect of thickness

Figs. 5–7 show R_p as a function of the C-layer thickness at different temperatures. The measurements obtained at −50 mV are d.c. measurements while those at OCV are impedance measurements. In the thickness range investigated, R_p decreases as the thickness increases. This implies some level of percolation in both the LSM and the YSZ for cathodes with a thickness up to 11 μm. It is unlikely that all existing

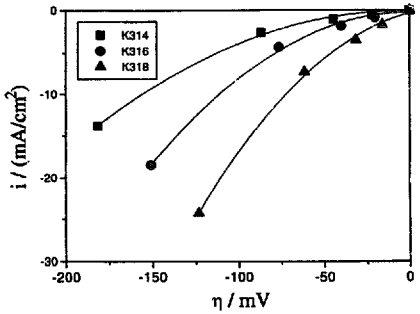

Fig. 4. i–η characteristics obtained in air at 700 °C. The curves are second-degree polynomials fit to the experimental values.

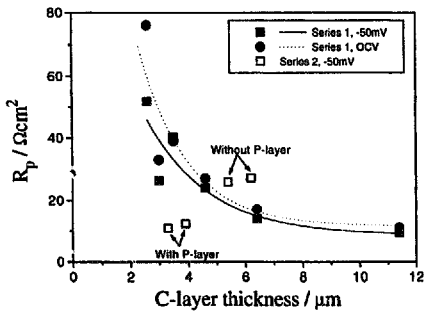

Fig. 5. Area specific polarisation resistance, R_p, determined in air at 700 °C plotted as a function of the C-layer thickness.

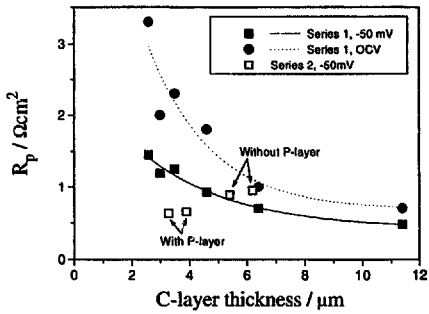

Fig. 6. Area specific polarisation resistance, R_p, determined in air at 850 °C plotted as a function of the C-layer thickness.

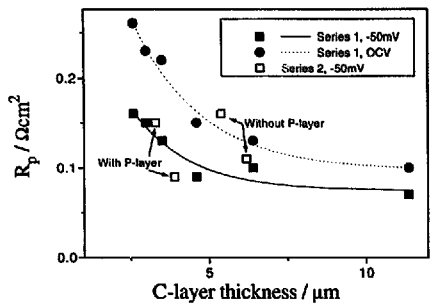

Fig. 7. Area specific polarisation resistance, R_p, determined in air at 1000 °C plotted as a function of the C-layer thickness.

TPB are active, due to limited percolation in one or more phases.

Looking at the absolute values in Figs. 5–7, the sensivity of R_p changes in the thickness of the layer was the highest at 700 and the lowest at 1000 °C. The data at 1000 °C (Fig. 7) were determined from extrapolation of the i–η characteristics. This may influence the accuracy, but does not explain the observed trend.

The relation between performance and temperature observed with d.c. measurements was confirmed by a.c. measurements. At low temperatures (700 and 850 °C) a majority of the impedance plots could be described by one dominant arc. However, what seems to be one dominant arc could actually be a number of overlapping arcs with similar time constants. At 1000 °C, four out of six impedance measurements were composed of two distinct arcs. Examples of the differences between impedance plots measured at varying temperatures are given in Fig. 8(a)–(c). It is uncertain what causes the presence of two distinct arcs in some impedance spectra. So far, no correlation between the number of arcs and the electrode thickness was found.

The apparent activation energy was not constant in the temperature range investigated, see Fig. 9. This may be due to the cathode reaction rate being limited by two or more reaction steps with different activation energies. The bulk of the electrochemical reaction might, therefore, not take place in the same volume fraction of the electrode at all temperatures, (see Section 3.3.1.). Furthermore, it is likely that the reaction zone along the active TPB is not the same at all measuring conditions [15]. The reaction zone is believed to expand into a broader band as the temperature increases.

The structural analysis by means of SEM revealed several trends. The micrographs in Fig. 10 and the following figures were obtained with backscattered electrons, i.e. the LSM phase looks brighter than the YSZ phase. The C-layers were generally dense and the porosity was not uniformly distributed, as illustrated in Fig. 10. A high fraction of the porosity was located between the C-layer and either the electrolyte or the CCC-layer. The amount of porosity tended to increase with the C-layer thickness. Adhesion of the C-layer to the electrolyte was extensive (Fig. 10).

Fig. 11 shows the C-layer being most similar to the expected ideal structure. Besides good electrochemical properties this sample had: (i) good adhesion to both the electrolyte and the CCC-layer; (ii) some percolation of LSM through the YSZ matrix, and (iii) porosity throughout the C-layer. An even higher porosity and a more uniform pore size distribution is expected to be preferable in ensuring percolation of gas through the C-layer, which could help to increase the active TPB length.

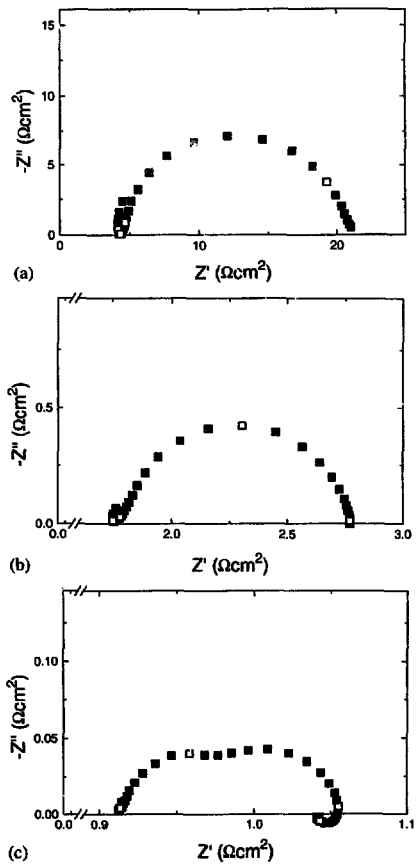

Fig. 8. Examples of impedance plots measured at OCV in air at varying temperatures, sample K317: (a) 700 °C; (b) 850 °C, and (c) 1000 °C. Data points at 10^{-2}, 1, 10^2 and 10^4 Hz are accentuated.

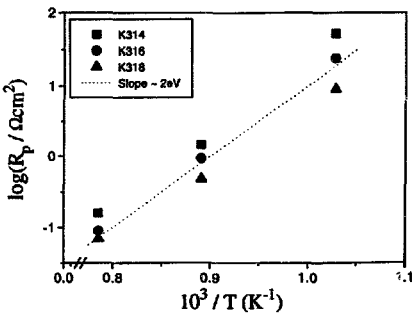

Fig. 9. Arrhenius plots obtained at −50 mV overvoltage in air, serie . 1. A reference line with a slope corresponding to an activation energy of ~ 2 eV is shown for comparison.

Fig. 10. SEM micrograph showing a cross section of sample K316 (series 1).

Fig. 11. SEM micrograph showing a cross section of sample K318 (series 1).

The results are comparable with data obtained by Kenjo and Nishiya [7]. They measured an area specific polarisation resistance of 0.16 Ω cm^2 for a LSM–YSZ composite electrode with equal amounts (by weight) of the two materials at 900 °C in air. The results obtained for sample K318 correspond to an R_p of approximately 0.22 Ω cm^2 at 900 °C in air (interpolated in Fig. 9). Also the effect of varying the thickness seems to be similar. Kenjo and Nishiya [7] painted and pressed iso-statically the green electrode. The electrodes in the present work were made by spray-coating, an easy technique to scale up and commercialise. This indicates that it is possible to manufacture electrodes with a good performance by industrial application methods.

3.2. Series 2, effect of P-layer

The results of series 2 are shown in Table 2. Application of a P-layer improves the performance at the lowest temperatures tested (700 and 850 °C). The observed effect cannot be explained by variations in the C-layer thickness, since the relationship between thickness and R_p was reversed in series 2 (Table 2). This is interpreted as the P-layer had a significant effect on R_p. As observed in series 1 the performance of series 2 was less dependent on the C-layer structure at 1000 °C than at lower temperatures. Comparing cathodes of similar thickness without a P-layer, cathodes prepared from partially precalcined LSM (series 1) have the lower R_p values (Figs 5–7). Thus, the sintering activity of LSM affects the performance.

Arrhenius plots for the samples of series 2, given in Fig. 12, show the same trend as observed for series 1.

The a.c. measurements showed the same tendencies as the d.c. measurements. In the impedance plots one dominant arc was observed at 700 and 850 °C. Fig. 13 shows impedance plots obtained at OCV and 1000 °C for the samples in series 2. Two distinct arcs were observed for samples with a P-layer while samples without a P-layer showed only one dominant arc. The origin of the second arc has not yet been fully investigated, but it suggests the rate limiting steps at 1000 °C depends on the microstructure.

For investigations of the structure, using SEM, two sintered TZ8Y tapes were sprayed with a P-layer (Fig. 14). One of the samples was additionally sprayed with a C-layer (Fig. 15). As shown in Fig. 14, the P-layer was inhomogeneous in thickness and particle size distribution. However, the largest particles were distributed in a mono-layer. This is preferable to a multi-layer, since a thin layer has a lower ohmic resistivity for ionic conduction through the P-layer.

Table 2
Results obtained for the samples of series 2 with or without a P-layer. The measuring conditions are −50 mV overvoltage in air. Each number is an average of two values. Values at 1000 °C are determined by extrapolation of the i–η characteristics

Sample	Temperature (°C)	C-layer thickness (µm)	R_p (−50 mV) (Ω cm^2)
With P-layer	704	3.6	12
Without P-layer		5.8	27
With P-layer	850	3.6	0.6
Without P-layer		5.8	0.9
With P-layer	1000	3.6	0.12
Without P-layer		5.8	0.14

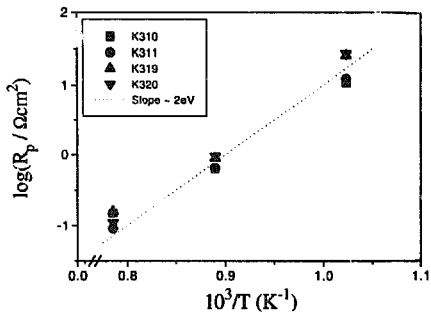

Fig. 12. Arrhenius plots obtained at −50 mV overvoltage in air, series 2. A reference line with a slope corresponding to an activation energy of −2 eV is shown for comparison.

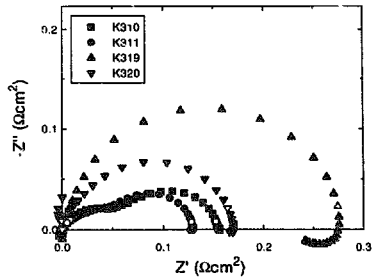

Fig. 13. Impedance plots measured at OCV and 1000 °C on samples with and without a P-layer (K310–K311 and K319–K320, respectively). The data are R_s-corrected. Data points at 1 and 10^4 Hz are accentuated.

Fig. 14. SEM micrograph showing a TZ8Y-tape with a sprayed and sintered P-layer.

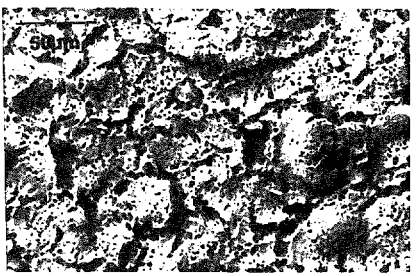

Fig. 15. SEM micrograph showing a TZ8Y-tape with a sprayed and sintered P-layer and C-layer.

Cracks were formed on the sample surface after the C-layer was sprayed and sintered (Fig. 15). The cracks are believed to originate through a combination of contractions while drying the electrode and shrinkage while firing. The C-layer appeared dense in certain areas, i.e. the porosity was inhomogeneously distributed.

In addition to the above-described structural examinations of samples mounted on tapes, the electrodes electrochemically investigated were also examined by SEM. The C-layer was most porous in samples with a P-layer, see Figs. 16 and 17. Additionally, the adhesion between the C-layer and the P-layer was good, but the number of contact points between the P-layer and the electrolyte was limited (Fig. 16). This increased the series resistance, but did not influence the polarisation resistance.

In the C-layer, YSZ tends to enclose the LSM particles (Fig. 17). Consequently, percolation through YSZ in the C-layer is more likely to occur than percolation through LSM. Therefore, the density of active TPB is assumed to be relatively high near the interface between the C-layer and the CCC-layer. On samples with a P-layer, the C-layer was broken into smaller islands rather than distributed in a continuous layer (Fig. 16). This formation of islands is expected to increase the contact area between the C-layer and the CCC-layer. The increased contact area in combination with the high density of TPB at the interface may explain the improvement in performance observed at 700 and 850 °C by application of a P-layer.

The application of a P-layer did not improve the performance at 1000 °C as observed at lower temperature. As discussed for series 1, this might be a consequence of an expansion of the reaction zone at high temperatures.

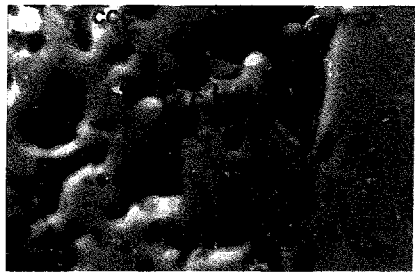

Fig. 16. SEM micrograph showing a cross section of an electrode with a P-layer (K311, series 2).

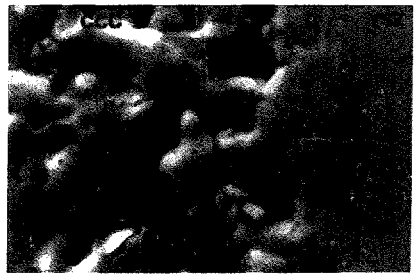

Fig. 17. SEM micrograph showing a cross section of an electrode without a P-layer (K320, series 2).

3.3. Models

Two simple models are used in order to estimate (i) the theoretical, active electrode thickness assuming percolation in the three phases through the C-layer and (ii) the potential for the improvement in the electrode structure. The models are based on the assumption tha the performance of a composite cathode correlates directly to the active TPB and depends mainly upon the TPB density, percolation and series resistance in the composite.

3.3.1. Model 1

The model displayed in Fig. 18 is used to estimate the active thickness of a composite cathode limited by ohmic resistance in the YSZ fraction. A YSZ cylinder stretches from the electrolyte surface through the composite electrode to the current collecting layer. In the model the contact points between the cylinder and the LSM grains create active TPB throughout the composite structure. The active thickness, t, of the composite structure is defined as the distance from the electrolyte where the polarisation resistance of one micrometer electrode, R'_p, equals the ionic resistance, R_{ion}, in the YSZ cylinder, i.e.:

$$R'_p = R_{ion} \tag{3}$$

The resistances in Eq. (3) are defined as follows:

$$R_{ion} = \frac{R_{YSZ,spec}\, t}{A} \tag{4}$$

$$R'_p = \frac{R_{p,spec}}{L'_{TPB}} \tag{5}$$

where $R_{YSZ,spec}$ is the specific resistance of YSZ, A is the cross-sectional area of the cylinder, $R_{p,spec}$ is the line-length specific reaction resistance of the TPB (Ω cm) and L'_{TPB} is the length of active TPB in 1 μm of the electrode. Eqs. (4) and (5) can be combined through Eq. (3), yielding the following expression for t:

$$t = \frac{R_{p,spec} A}{R_{YSZ,spec} L'_{TPB}} \tag{6}$$

A cylinder diameter, $2r$, of 2 μm and a L'_{TPB} of πr μm are estimated from the micrographs. The value $R_{p,spec} = 150$ Ω cm is a rough estimate taken from Juhl et al. [16]. This value was measured with a point electrode, where the oxygen reduction reaction is assumed to occur along the perimeter of the contact area. Using an $R_{YSZ,spec}$ of 10 Ω cm [17] at 1000 °C the model yields an active thickness, t, of 15 μm. This is in good agreement with experimental findings.

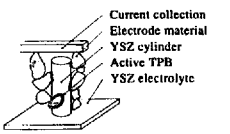

Fig. 18. Simple model illustrating the limitation of the active thickness of a composite electrode by resistance in a YSZ cylinder.

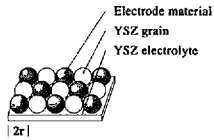

Fig. 19. Simple model illustrating the density of the triple phase boundary in an ordered composite consisting of a monolayer of particles.

Estimating t at different temperatures, the apparent activation energies of −0.8 eV for $R_{YSZ,spec}$ [18] and −2 eV for $R_{p,spec}$ [15] are considered appropriate. Using 15 μm at 1000 °C as a reference value, the active thickness, t, is 60 μm at 850 °C and 400 μm at 700 °C, respectively.

The measured R_p values are apparently constant for C-layer thicknesses above 10 μm (Figs. 5–7). Compared with the calculations above this was not expected at 700 and 850 °C. One reason for this behaviour might be a lack of electron and gas percolation paths through the entire C-layer thickness. Consequently, parameters other than ionic resistance in the YSZ phase could be a limiting factor.

The observed insensitivity to structural changes at 1000 °C compared with lower temperatures could, according to Eq. (6), be related to changes in the ratio between $R_{p,spec}$ and $R_{YSZ,spec}$ with temperature, due to different activation energies. Thus, the experimental findings may be qualitatively explained by a change in active thickness.

3.3.2. Model 2

A theoretical L_{TPB} in a mono-layer is calculated in order to evaluate the performance which may be achieved for a composite cathode. An ideal-ordered mono-layer consisting of LSM and YSZ (ratio 1:1) is sketched in Fig. 19. A mono-layer with spheres of 2 μm is assumed to have 5/2 contacts per sphere, each with an ideal TPB length of 2 μm, giving an L_{TPB} of 1.25×10^4 cm/cm^2 for the mono-layer. Using this value in Eq. (5) and maintaining $R_{p,spec}$ yields an area specific polarisation resistance, R_p, of 0.01 Ω cm^2 at 1000 °C for the 2 μm mono-layer. Comparing this value to the best LSM–YSZ composite cathodes having R_p values of 0.1–0.14 Ω cm^2 for 3–6 μm thickness at 1000 °C indicates a considerable potential for improving performance by controlling the structure.

4. Conclusions

At low temperatures (700 and 850 °C) increasing the layer thickness of a composite cathode had a positive effect on the electrode performance in the range of thicknesses investigated. This implies that the bulk of the LSM–YSZ composite cathode is active with respect to the oxygen reduction reaction. At 1000 °C the polarisation resistance was less sensitive to variations in thickness than at lower temperature.

The application of a porous layer of YSZ particles between the electrolyte and the composite cathode decreased the polarisation resistance at 700 and 850 °C, whereas no significant effect was observed at 1000 °C. The particle layer is believed to have extended the active triple phase boundary length locally at the interface between the composite cathode and the LSM current collecting layer.

The results suggest that with the materials and application method used, the largest potential for performance improvement by controlling the microstructure and thickness lies at temperatures well below 1000 °C. Thus, these results can be utilised in relation to lowering the operation temperature of SOFCs.

Two simple models to estimate the theoretical active thickness and the minimal obtainable polarisation resistance have been used. Although the two proposed models are simplified, they point out the potential in optimisation of the electrode structure and thickness. The key to considerable improvement of the microstructure is to obtain a uniform blend of the three phases in the C-layer (LSM, YSZ and pores), leading to percolation of electrons, oxide ions and gas through the C-layer, since this will extend the active triple phase boundary line. Both the experimental and the theoretical part of the present work implies that large improvements in performance of composite electrodes are within reach.

Acknowledgements

The presented work was carried out as a part of the JOULE 2 project 'New SOFC Materials and Technology', Contract JOU2-CT92-0063. Co-workers from the SOFC group at the Materials Department, Risø National Laboratory are gratefully acknowledged for the production of samples. Senior Scientist Carsten Bagger and Dr Nicholas Bonanos, both at Risø National Laboratory, are acknowledged for valuable discussions.

References

[1] F.A. Kröger and H.J. Vink, *Solid State Physics, 3* (1956) 307.
[2] J. Mizusaki, H. Tagawa, K. Tsuneyoshi, K. Mori and A. Sawata, *Nippon Kagaku Kaishi*, (1988) 1623.
[3] J. Mizusaki, H. Tagawa, K. Tsuneyoshi and A. Sawata, *J. Electrochem. Soc., 138* (1991) 1867.
[4] K. Sasaki, J.P. Wurth, M. Gödickemeier, A. Mitterdorfer and L.J. Gauckler, *Proc. 4th Int. Symp. SOFC, Yokohama, Japan, 1995*, p. 625.
[5] F.H. van Heuveln, F.P.F. van Berkel and J.P.P. Huijsmans, *Proc. 14th Risø Int. Symp. Materials Sciences, Roskilde, Denmark, 1993*, p. 53.
[6] L.G.J. de Haart, R.A. Kuipers, K.J. de Vries and A.J. Burggraf, *J. Electrochem Soc., 138* (1991) 1970.
[7] T. Kenjo and M. Nishiya, *Solid State Ionics, 57* (1992) 295.
[8] M.J.L. Østergård, C. Clausen, C. Bagger and M. Mogensen, *Electrochim. Acta, 40* (1995) 1971.
[9] C. Clausen, C. Bagger, J.B. Bilde-Sørensen and A. Horsewell, *Solid State Ionics, 70/71* (1994) 59.
[10] J.A.M. van Roosmalen and E.H.P. Cordfunke, *Solid State Ionics, 52* (1992) 303.
[11] L.A. Chick, L.R. Pederson, G.D. Maupin, J.L. Bates, L.E. Thomas and G.J. Exarhos, *Mater. Lett., 10* (1990) 6.
[12] N. Christiansen and P. Gordes, *Proc. 2nd Int. Symp. SOFC, Athens, Greece, 1991*, p. 495.
[13] C. Bagger, B. Kindl and M. Mogensen, *Patent Applic., Publication No. WO94/20998*.
[14] B.A. Boukamp, *Solid State Ionics, 20* (1986) 31.
[15] M. Kleitz, T. Kloidt and L. Dessemond, *Proc. 14th Risø Int. Symp. Materials Sciences, Roskilde, Denmark, 1993*, p. 89.
[16] M. Juhl, M. Mogensen, T. Jacobsen, B. Zachau-Christiansen, N. Thorup and E. Skou, *Proc. 4th Int. Symp. SOFC, Yokohama, Japan, 1995*, p. 554.
[17] F.T. Ciacchi, K.M. Crane and S.P.S. Badwal, *Solid State Ionics, 73* (1994) 49.
[18] D.K. Hohnke, in P. Vashishta, J.N. Mundy and G.K. Shenoy (eds.), *Proc. Int. Conf. Fast Ion Transport in Solids, Lake Geneva, WI, USA, 1973*, Elsevier, Amsterdam, 1979, p. 669.